Aerosol Size Distributions Obtained by Inversion of Spectral Optical Depth Measurements

MICHAEL D. KING,[1,4] DALE M. BYRNE,[2,5] BENJAMIN M. HERMAN[1] AND JOHN A. REAGAN[3]

The University of Arizona, Tucson 85721

(Manuscript received 17 February 1978, in final form 15 August 1978)

ABSTRACT

Columnar aerosol size distributions have been inferred by numerically inverting particulate optical depth measurements as a function of wavelength. An inversion formula which explicitly includes the magnitude of the measurement variances is derived and applied to optical depth measurements obtained in Tucson with a solar radiometer. It is found that the individual size distributions of the aerosol particles (assumed spherical), at least for radii $\gtrsim 0.1$ μm, fall into one of three distinctly different categories. Approximately 50% of all distributions examined thus far can best be represented as a composite of a Junge distribution plus a distribution of relatively monodispersed larger particles centered at a radius of about 0.5 μm. Scarcely 20% of the distributions yielded Junge size distributions, while 30% yielded relatively monodispersed distributions of the log-normal or gamma distribution types. A representative selection of each of these types will be presented and discussed. The sensitivity of spectral attenuation measurements to the radii limits and refractive index assumed in the numerical inversion will also be addressed.

1. Introduction

A relationship between the size of atmospheric aerosol particles and the wavelength dependence of the extinction coefficient was first suggested by Ångström (1929). Since that time Ångström's (1929) empirical formula for the wavelength dependence of the extinction coefficient has been directly related to a parameter of a Junge size distribution when the radii extend from 0 to ∞ (van de Hulst, 1957; Junge, 1963). Curcio (1961) used the wavelength dependence of the particulate extinction coefficient in the visible and near-infrared regions to infer the aerosol size distributions existing above water in the Chesapeake Bay area. He determined that the majority of aerosol size distributions could best be represented by a two-component size distribution consisting of a Junge-type distribution plus a small component of larger particles. This type of composite distribution was the most capable of explaining the wavelength dependence of the attenuation measurements he observed.

Yamamoto and Tanaka (1969) were the first to apply a numerical inversion algorithm to spectral measurements of extinction coefficient in order to determine an aerosol size distribution. These authors applied the linear inversion techniques developed by Phillips (1962) and Twomey (1963) to the problem of numerically solving the Fredholm integral equation of the first kind which arises in this problem. Although they clearly demonstrated that these numerical procedures are quite successful for obtaining size distributions by remote sensing, other investigators more recently have still continued to estimate parameters of model size distributions from spectral attenuation measurements (e.g., Quenzel, 1970; Shaw *et al.*, 1973). Although these fitting procedures are reasonably satisfactory, they are more restrictive than inversion procedures in that they assume that the atmospheric particulates follow one of several possible analytical distributions.

Grassl (1971) presents an iterative method for numerically inverting spectral attenuation data. After demonstrating the success of this algorithm on spectral attenuation coefficients generated for three model size distributions, the size distributions obtained by inversion of two real data cases are presented. In order to accurately determine aerosol size distributions from spectral optical depth measurements obtained from direct solar observations, it is necessary to collect optical depth measurements over a sufficient number of wavelengths to obtain a good estimate of both the ozone absorption and particulate optical depths

[1] Institute of Atmospheric Physics.
[2] Optical Sciences Center.
[3] Department of Electrical Engineering.
[4] Present affiliation: Goddard Space Flight Center, Greenbelt, MD 20771.
[5] Present affiliation: Pratt & Whitney Aircraft, Government Products Division, Box 2691, West Palm Beach, FL 33402.

0022-4928/78/2153-2167$07.50

separately. In making these corrections, Grassl (1971) used tabulated values for a model atmosphere in lieu of alternative observations.

In the present investigation an earlier theoretical study (Herman *et al.*, 1971) of angular scattering intensities has been extended to the problem of inferring columnar aerosol size distributions by inversion of spectral optical depth measurements. An inversion formula which explicitly includes the magnitudes of the measurement variances is derived and applied to optical depth measurements obtained in Tucson with a solar radiometer. Aerosol size distribution results have been obtained for 57 days and the results of a representative selection are presented, together with a discussion of the relative frequency of occurrence of various types of distributions. Some of the practical difficulties to be considered when inverting spectral attenuation measurements will be discussed. The most important of these are the radii limits of maximum sensitivity and the particulate refractive index assumed in the inversion.

2. Method of solution

From wavelength measurements of the directly transmitted solar flux density as a function of solar zenith angle, one can obtain spectral values of the particulate (Mie) optical depth (Shaw *et al.*, 1973; King and Byrne, 1976). The spectral variation of Mie optical depth, designated $\tau_M(\lambda)$, is produced through attenuation by aerosol and is primarily determined by the aerosol size distribution. Assuming that the atmospheric particulates can be modeled by equivalent spheres of known refractive index to a sufficient degree of accuracy, the integral equation which relates optical depth to an aerosol size distribution can be written as

$$\tau_M(\lambda)=\int_0^\infty\int_0^\infty \pi r^2 Q_{\text{ext}}(r,\lambda,m)n(r,z)dzdr, \qquad (1)$$

where $n(r,z)dr$ is the height-dependent aerosol number density in the radius range r to $r+dr$; m the complex refractive index of the aerosol particles; λ the wavelength of the incident illumination; and $Q_{\text{ext}}(r,\lambda,m)$ the extinction efficiency factor from Mie theory. The effects of possible variations of the particulate refractive index with wavelength and particle radius will be discussed in Section 4. In the present formulation, the aerosol is assumed to consist of homogeneous spherical particles which are nondispersive over the wavelength range of the observations. Performing the height integration, Eq. (1) can be rewritten as

$$\tau_M(\lambda)=\int_0^\infty \pi r^2 Q_{\text{ext}}(r,\lambda,m)n_c(r)dr, \qquad (2)$$

where $n_c(r)$ is the unknown columnar aerosol size distribution, i.e., the number of particles per unit area per unit radius interval in a vertical column through the atmosphere.

To determine $n_c(r)$, the transform of (2) must be obtained. Since an expression for $n_c(r)$ cannot be written analytically as a function of the $\tau_M(\lambda)$ values, a numerical approach must be followed. Therefore, the integral in (2) is replaced by a summation over coarse intervals in r, each of which is composed of several subintervals as described by Herman *et al.* (1971) for the case of the angular distribution of scattered light of one wavelength. In order to examine the specific kernel functions which result if that procedure is applied to the present problem, we let $n_c(r)=h(r)f(r)$, where $h(r)$ is a rapidly varying function of r, while $f(r)$ is more slowly varying. With this substitution, Eq. (2) becomes

$$\tau_M(\lambda)=\int_{r_a}^{r_b}\pi r^2 Q_{\text{ext}}(r,\lambda,m)h(r)f(r)dr$$

$$=\sum_{j=1}^{q}\int_{r_j}^{r_{j+1}}\pi r^2 Q_{\text{ext}}(r,\lambda,m)h(r)f(r)dr, \qquad (3)$$

where the limits of integration have been made finite with $r_1=r_a$ and $r_{q+1}=r_b$. If $f(r)$ is assumed constant within each coarse interval, a system of linear equations results which may be written as

$$\mathbf{g}=\mathbf{A}\mathbf{f}+\boldsymbol{\varepsilon}, \qquad (4)$$

where $\boldsymbol{\varepsilon}$ is an unknown error vector whose elements ϵ_i represent the deviation between measurement (g_i) and theory ($\sum_j A_{ij}f_j$). This deviation arises from quadrature and measurement errors, as well as any uncertainties as to the exact form of the kernel function [in this case, $\pi r^2 Q_{\text{ext}}(r,\lambda,m)$].

Returning to (3), it follows that the elements of (4) are given by

$$g_i=\tau_M(\lambda_i), \qquad i=1, 2, \ldots, p,$$

$$A_{ij}=\int_{r_j}^{r_{j+1}}\pi r^2 Q_{\text{ext}}(r,\lambda_i,m)h(r)dr, \quad j=1, 2, \ldots, q, \qquad (5)$$

$$f_j=f(\bar{r}_j),$$

where $\bar{r}_j$ are the midpoints of the coarse intervals. Writing (5) as a quadrature results in an expression similar to that obtained by Herman *et al.* (1971) where their weighting functions $W_{k_j}(r_{k_j})=h(r_{k_j})\Delta r_{k_j}$ in the terminology used here and r_{k_j} are the midpoint radii of the subintervals.

In terms of an integral over $x=\log r$, Eq. (5) may be rewritten as

$$A_{ij}=\int_{x_j}^{x_{j+1}}K(x,\lambda_i)dx, \qquad (6)$$

where

$$K(x,\lambda)=\pi 10^{3x}Q_{\text{ext}}(10^x,\lambda,m)\,h(10^x)\ln 10. \quad (7)$$

Eqs. (6) and (7) are those obtained by Yamamoto and Tanaka (1969) if $h(r)$ takes the form of a Junge (1955) size distribution,

$$h(r)=r^{-(\nu^*+1)}, \quad (8)$$

with ν^* assumed to have a value of 3.0.

Phillips (1962) and Twomey (1965) have discussed the instability in the solution vector $\mathbf{f}$ which results if (4) is directly solved by minimizing $\sum_i \epsilon_i^2$. Phillips suggested that, due to ever-present error, a constraint be added that discriminates against such instability. In order to select a physical solution among the family of solutions which satisfy (4), Phillips introduced a smoothing constraint such that the sum of the squares of the second derivatives of the solution points is minimized. For a quadrature of equal division, the solution vector $\mathbf{f}$ is obtained by minimizing a performance function Q, defined as

$$Q=\sum_{i=1}^{p}\epsilon_i^2+\gamma\sum_{j=2}^{q-1}(f_{j-1}-2f_j+f_{j+1})^2, \quad (9)$$

where γ is some non-negative Lagrange multiplier. Minimizing Q with respect to the unknown f_k coefficients, when γ equals zero, is equivalent to making an unweighted least-squares fit to the data.

Since it is further known that some of the $\tau_M(\lambda_i)$ measurements are more precise than others, it is desirable to include that *a priori* information in the mathematical formalism. For the case in which the measurements are correlated with known covariances $\sigma^2_{\tau_i\tau_j}$, a more general form of (9) would be

$$Q=\sum_{i=1}^{p}\sum_{j=1}^{p}C_{ij}^{-1}\epsilon_i\epsilon_j+\gamma\sum_{j=2}^{q-1}(f_{j-1}-2f_j+f_{j+1})^2, \quad (10)$$

where C_{ij} is an element of the measurement covariance matrix $\mathbf{C}$ whose elements are given by $C_{ij}=\sigma^2_{\tau_i\tau_j}$. This follows from the Gauss–Markov theorem in the absence of a constraint (see, e.g., Liebelt, 1967), and thus the minimum value of Q represents the statistically optimum estimate of $\mathbf{f}$.

Following the method suggested by Twomey (1963) whereby the performance function is differentiated with respect to each of the f_k coefficients, a set of simultaneous equations results which may be written as

$$-\sum_{i=1}^{p}\sum_{j=1}^{p}C_{ij}^{-1}A_{ik}\epsilon_j+\gamma\sum_{j=1}^{q}H_{kj}f_j=0, \qquad k=1,2,\ldots,q, \quad (11)$$

where H_{kj} is an element of the smoothing matrix $\mathbf{H}$ defined by Twomey (1963) as

$$\mathbf{H}=\begin{bmatrix} 1 & -2 & 1 & 0 & 0 & & & & \\ -2 & 5 & -4 & 1 & 0 & 0 & & & \\ 1 & -4 & 6 & -4 & 1 & 0 & & & \\ 0 & 1 & -4 & 6 & -4 & 1 & 0 & & \\ & & & \ddots & & & & & \\ & & & & 0 & 1 & -4 & 5 & -2 \\ & & & & & 0 & 1 & -2 & 1 \end{bmatrix}. \quad (12)$$

The series of equations in (11) can be written in matrix form as

$$-\mathbf{A}^{\mathrm{T}}\mathbf{C}^{-1}\boldsymbol{\epsilon}+\gamma\mathbf{H}\mathbf{f}=0, \quad (13)$$

where $\mathbf{A}^{\mathrm{T}}$ is the transpose of $\mathbf{A}$. Eliminating $\boldsymbol{\epsilon}$ between (4) and (13) leads to the solution

$$\mathbf{f}=(\mathbf{A}^{\mathrm{T}}\mathbf{C}^{-1}\mathbf{A}+\gamma\mathbf{H})^{-1}\mathbf{A}^{\mathrm{T}}\mathbf{C}^{-1}\mathbf{g}. \quad (14)$$

For the case in which the statistical errors in the measurements are assumed equal and uncorrelated, $\mathbf{C}$ reduces to $s^2\mathbf{I}$, where s represents the constant rms error and $\mathbf{I}$ is the identity matrix. With this assumption, Eq. (14) reduces to the form derived by Twomey (1963).

For the attenuation problem considered here, the statistical errors in the measurements are assumed uncorrelated but known to be unequal (King and Byrne, 1976). As a consequence of this, the covariance matrix becomes diagonal with elements given by $C_{ij}=\sigma^2_{\tau_M}(\lambda_i)\delta_{ij}$, where δ_{ij} is the Kronecker delta function. This gives a relative weighting to each of the measurements, placing greater emphasis on those measurements which have the smallest error bars. With $\mathbf{C}$ defined in this manner, Eq. (14) is equivalent to making a weighted least-squares fit to the data subject to a constraint.

Initially, a zeroth-order weighting function $h^{(0)}(r)$ is assumed in (5) from which first-order $f^{(1)}(\bar{r}_j)$ values are computed with the aid of (14). Since the solution vector $\mathbf{f}^{(1)}$ represents a modifying factor to the assumed form of $h^{(0)}(r)$, the $f^{(1)}(\bar{r}_j)$ values are then used to calculate a first-order weighting function, $h^{(1)}(r)$, which better represents the size distribution than the initially assumed weighting function. The first-order weighting function is then substituted back into (5) from which a second-order $\mathbf{f}^{(2)}$ is obtained through (14). This iterative procedure is continued until a stable result is obtained (Herman *et al.*, 1971).

Two advantages result from separating the size distribution function into two parts as described above. The most obvious advantage is that the quadrature error which results from (3), when $f(r)$ is assumed constant in each coarse interval, will be less the better $h(r)$ comes to describing the size distribution. In fact, if the weighting function represents the size distribution exactly, $\mathbf{f}$ will be a vector whose elements are unity (Herman *et al.*, 1971). The second advantage, though less obvious, is equally important. Since the smoothing constraint minimizes the second derivatives

of the solution points on a *linear* scale, it is a much more appropriate constraint in cases in which $f(\bar{r}_j)$ is nearly constant. Since the columnar size distribution typically varies over many orders of magnitude, a direct inversion for $n_c(r)$ would consist of minimizing curvature of a function which implicitly has large curvature. A Junge distribution, for example, is nearly a delta function for large values of ν^* on a linear scale and hence has large curvature, even though it has zero curvature on a log scale (Twomey, personal communication).

For the results presented in this paper, the initial weighting functions were assumed to have the form of a Junge size distribution given by (8). In practice, several different values of ν^* are used to calculate the zeroth-order weighting function and the final results after successive iterations are intercompared. One test of the procedure is the similarity of the results obtained when different values of ν^* are used. This point will further be addressed in the next section.

In performing the inversion described above, it is necessary to select a value for γ. Since γ enters (14) in a manner such that elements of $\gamma\mathbf{H}$ are to be added to $\mathbf{A}^T\mathbf{C}^{-1}\mathbf{A}$ to produce the desired smoothing, the magnitude of $\gamma H_{kj}/(\mathbf{A}^T\mathbf{C}^{-1}\mathbf{A})_{kj}$ is of importance, not the magnitude of γ alone. In selecting γ, therefore, $\gamma_{\text{rel}} \equiv \gamma H_{11}/(\mathbf{A}^T\mathbf{C}^{-1}\mathbf{A})_{11}$ is allowed to vary in the range 10^{-3} to 1 until a minimum value of γ_{rel} is reached for which all elements of the solution vector $\mathbf{f}$ are positive (i.e., negative values of the elements of $\mathbf{f}$ constitute an unphysical solution).

3. Aerosol size distribution results

The method for determining the columnar aerosol size distribution described in the preceding section has been carried out at the University of Arizona since August 1975. The Mie optical depth measurements have been determined by the method described by King and Byrne (1976). In this procedure the ozone absorption optical depths, and hence total ozone content of the atmosphere, are inferred from the spectral variation of total optical depth in the visible and near infrared wavelength regions. Using the O_3 absorption optical depths determined in this manner, the values of the Mie optical depth are obtained by subtracting the molecular scattering and estimated O_3 absorption contributions from the total optical depth. At the present time inversions have been carried out for 57 different days, of which the results of a representative selection are presented below. For consistency of presentation, all inversions were performed assuming the complex refractive index of the aerosol particles was wavelength and size independent and given by $m=1.45-0.00i$. Although this value was arbitrarily selected, there is considerable evidence that the real part of the index of refraction lies somewhere between 1.33 (pure water) and 1.54 (silicate particles) as discussed by Yamamoto and Tanaka (1969) and others. The results of a combined direct sampling and remote sensing experiment over Tucson in November 1974 are suggestive of a real index between 1.40 and 1.45 for the aerosol particles (Reagan *et al.*, 1977). This refractive index is in good agreement with the refractive index of $H_2SO_4 \cdot b\ H_2O$ droplets which comprised about 30% of the particles analyzed by the electron microscope in this experiment (Reagan *et al.*, 1977). The effect of varying the refractive index assumed in the inversion procedure was addressed by Yamamoto and Tanaka (1969) where it was shown that the inverted size distribution maintains its *shape* under various values of refractive index when $m \approx 1.0$. The validity of this result for indices of refraction between 1.45 and 1.54 will be examined in Section 4.

Optical depth measurements made at between six and eight different wavelengths ranging between 0.4400 and 1.0303 μm have been used in the size distribution determinations to be presented below. Due to both the extinction cross sections (which increase significantly with radius) and the number densities of the natural aerosol particles (which normally decrease with radius), this spectral region of the attenuation measurements limits the radius range of maximum sensitivity to the large and giant aerosol particles only ($0.1 \lesssim r \lesssim 4.0$ μm). Although this matter has been considered by Yamamoto and Tanaka (1969) for both Junge- and Woodcock-type aerosol size distributions, it is very important to realize that there is no absolute rule which determines the radii limits having the most significant contribution to the attenuation measurements. As will be shown in the next section, this radius range is dependent on both the form of the size distribution function and the values of the Mie extinction cross sections over the radius range. Since the size distribution function is not known in advance, it is apparent that occasional trial and error is required in order to determine the radius range over which the inversion can be performed.

It is convenient, for purposes of illustration, to categorize the inversion results according to both the form of the columnar aerosol size distribution and the spectral dependence of the Mie optical depths. In lieu of $n_c(r)$ or, equivalently, dN_c/dr, the size distribution results are presented in terms of $dN_c/d\log r$, representing the number of particles per unit area per unit log radius interval in a vertical column through the atmosphere. In most cases the columnar aerosol size distributions can be classified in terms of three different types of distributions (although gradations between two different types are occasionally observed making this classification somewhat arbitrary). An example of the first type is illustrated in Fig. 1 for 13 August 1975, a day for which the spectral Mie optical depth measurements very nearly follow Ångström's (1929) empirical formula given by $\tau_M(\lambda) = \beta\lambda^{-\alpha}$. The observed Mie optical depths and corresponding standard devia-

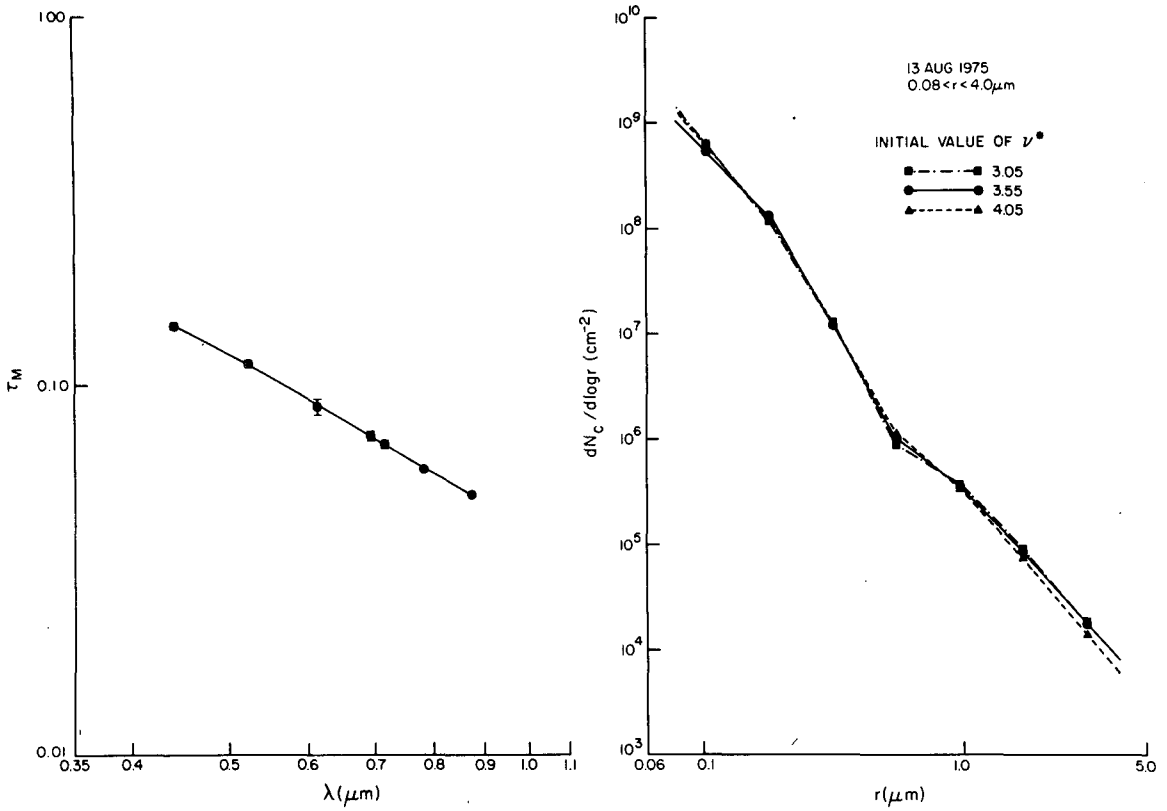

FIG. 1. Observed Mie optical depths and estimated size distributions for 13 August 1975. The three distribution curves on the right represent the results using different initial weighting functions (see text) while the curve on the left indicates the regression fit to the data using the inverted size distributions.

tions are shown in the left portion of the figure while the size distributions obtained by inverting these data for three initial ν^* cases are shown in the right portion. The solid curve in the left portion indicates how the inverted size distributions are able to reproduce the $\tau_M(\lambda)$ measurements (i.e., the direct problem $\mathbf{g}=\mathbf{Af}$).

In applying the inversion procedure described in the preceding section, several different initial Junge distribution parameters ν^* are assumed in formulating the zeroth-order weighting functions $h^{(0)}(r)$ so that the results after subsequent iterations can be intercompared. In practice, a best-fit value for the Ångström turbidity coefficient α is determined from the observed values of $\tau_M(\lambda)$ by linear least-squares methods, from which a corresponding ν^* value is determined from the well-known relationship $\nu^*=\alpha+2$. Inversions are then performed for three different values of the Junge parameter about this value (*viz.*, $\nu^*-0.5$, ν^* and $\nu^*+0.5$). For the data case illustrated in Fig. 1 $\alpha=1.55$, and thus inversions were performed using the initial values $\nu^*=3.05$, 3.55 and 4.05 as indicated in the right-hand figure. It is readily apparent that all initial values of the weighting functions $h^{(0)}(r)$ were able to be perturbed such that the results after subsequent iterations yielded solutions quite independent of the initial "guess."

The aerosol size distributions illustrated in Fig. 1 can best be described as constituting either Junge or two-slope types of size distributions. They have been observed on approximately 20% of all days examined thus far. Fig. 2 illustrates the spectral optical depth measurements and corresponding size distributions for three additional days (7 and 29 August and 29 October, 1975) where only one distribution function is shown for each day. In all instances the sensitivity to the initial weighting function $h^{(0)}(r)$ was negligible. The Mie optical depth data for cases of this type always tend to exhibit linear or slightly positive curved spectral dependences of $\log\tau_M(\lambda)$ vs $\log\lambda$ with relatively steep slopes ($\alpha\approx1.2$) and relatively high turbidities [$\tau_M(0.6120\,\mu\text{m})\approx0.08$]. The one-to-one correspondence between the slope of the data (α) and the slope of the inverted size distribution (ν^*) is readily apparent on examination of Fig. 2.

On occasions when the Mie optical depths are small, $\tau_M(\lambda)$ tends generally to increase with wavelength (i.e., $\alpha<0.00$). On most of these occasions the spectral Mie optical depth measurements exhibit negative curvature. An example of this type is illustrated in Fig. 3 for the data of 24 October 1975. In a similar manner to the method described above, an Ångström turbidity coefficient was estimated from the data to be

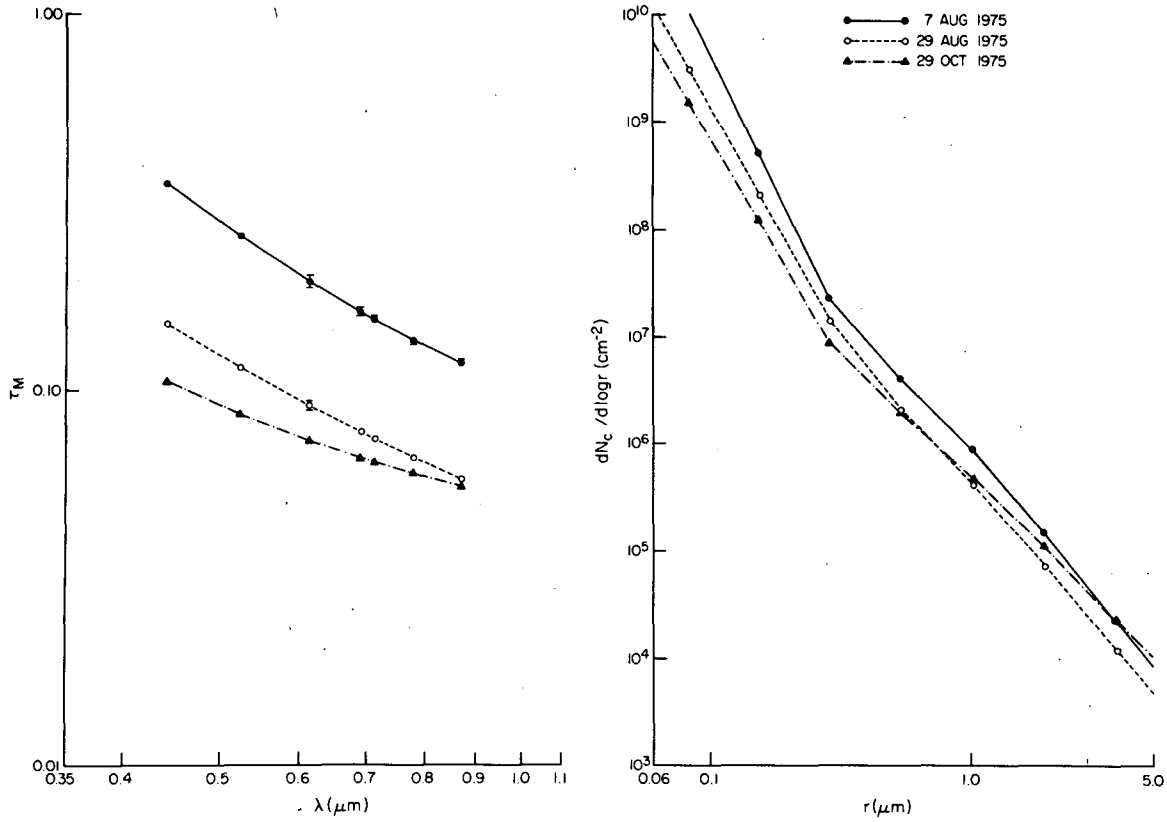

FIG. 2. Observed Mie optical depths and estimated size distributions for 7 August, 29 August and 29 October, 1975.

$\alpha = -0.27$, and thus inversions were performed using weighting functions having initial Junge parameters $\nu^* = 1.23$, 1.73 and 2.23. It is readily apparent on examination of Fig. 3 that distinctly non-Junge size distributions result from data of this type. This is not unexpected since the tendency for negative curvature on the part of the data suggests an absence of both small and large particles.

The three different size distributions illustrated in Fig. 3 indicate a relative insensitivity to the choice of the Junge parameter in the initial weighting functions except in the radius range where little retrievable information exists. The inversion result presented here was specifically selected because it clearly demonstrates that the inversion procedure is capable of perturbing the initial guess as required. Most data (but not all) do not necessitate such a drastic alteration of the initial weighting function $h^{(0)}(r)$. All days for which the Mie optical depths exhibit negative curvature while increasing with wavelength produce inverted size distributions which are relatively monodisperse, as is the case with the data of Fig. 3. These types of distributions have been observed on approximately 30% of all days examined thus far.

Fig. 4 illustrates the spectral optical depth measurements and corresponding size distributions for 12 November 1975 and 6 and 15 May 1977, days for which the $\tau_M(\lambda)$ data increase with wavelength. In all instances the inverted size distributions are relatively monodisperse in character with very little sensitivity to the initial weighting function $h^{(0)}(r)$. Data of this type are often difficult to invert due to the problems associated with determining the radius range having the major contribution to the attenuation measurements. For this reason it is frequently necessary to invert a data set several different times with slight alterations in the radius range. To this end, the agreement between distributions having different initial weighting functions affords a very convenient subjective test of stability. None of the attenuation measurements over the Chesapeake Bay (Knestrick *et al.*, 1962) which were considered by Yamamoto and Tanaka (1969) showed any spectral dependencies similar to Figs. 3 and 4. The large Junge parameter ($\nu^* = 3.0$) used in their weighting functions would probably have made it more difficult to invert any data of this type had they occurred.

Not all spectral optical depth measurements which exhibit negative curvature or negative Ångström turbidity coefficients [i.e., $\tau_M(\lambda)$ increases as a function of λ] show quite as dramatic a monodisperse character to the size distributions as the data of Figs. 3 and 4. Fig. 5 illustrates the spectral optical depth measurements and corresponding size distributions for 10 October

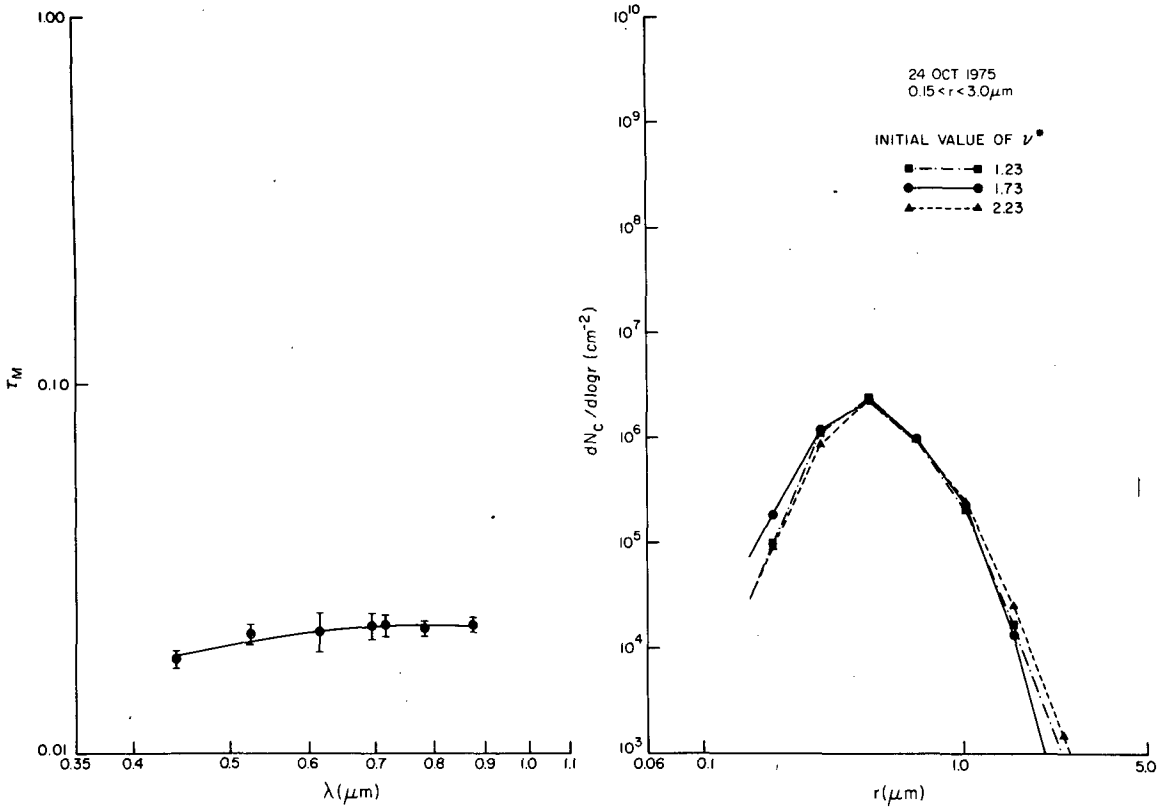

FIG. 3. As in Fig. 1 except for measurements collected on 24 October 1975.

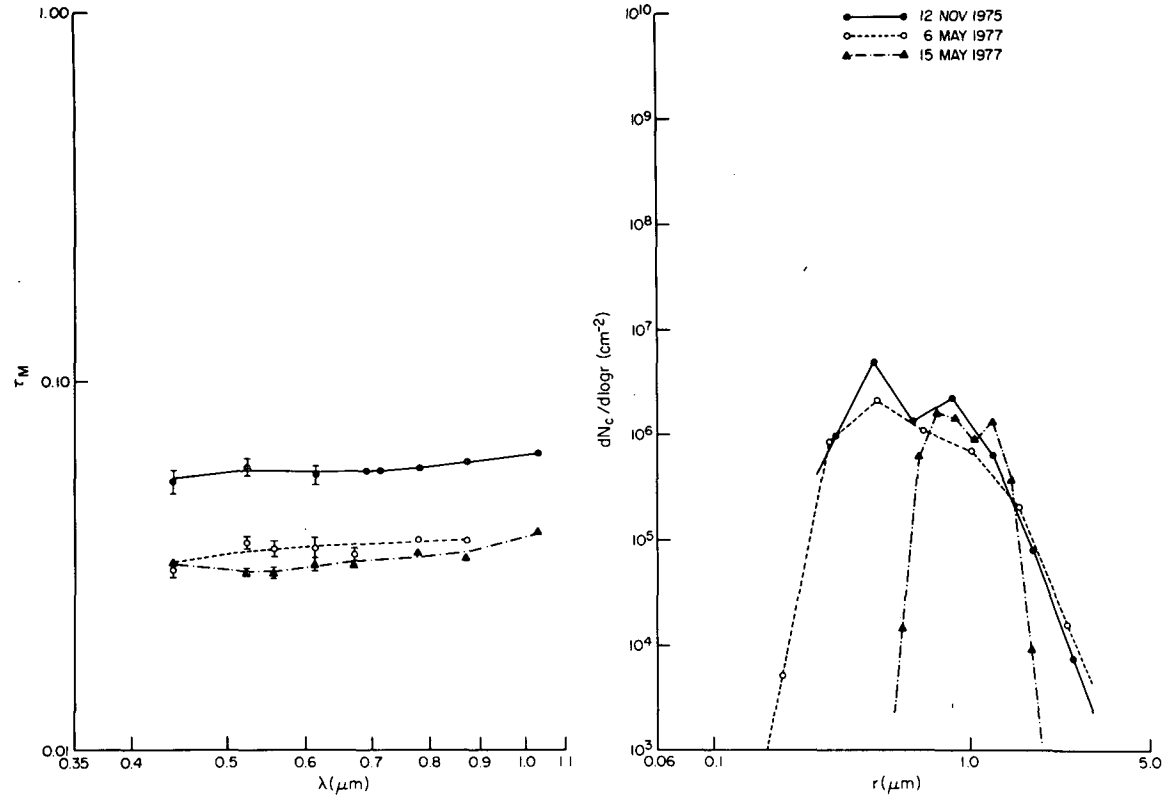

FIG. 4. As in Fig. 2 except for measurements on 12 November 1975, 6 May 1977 and 15 May 1977.

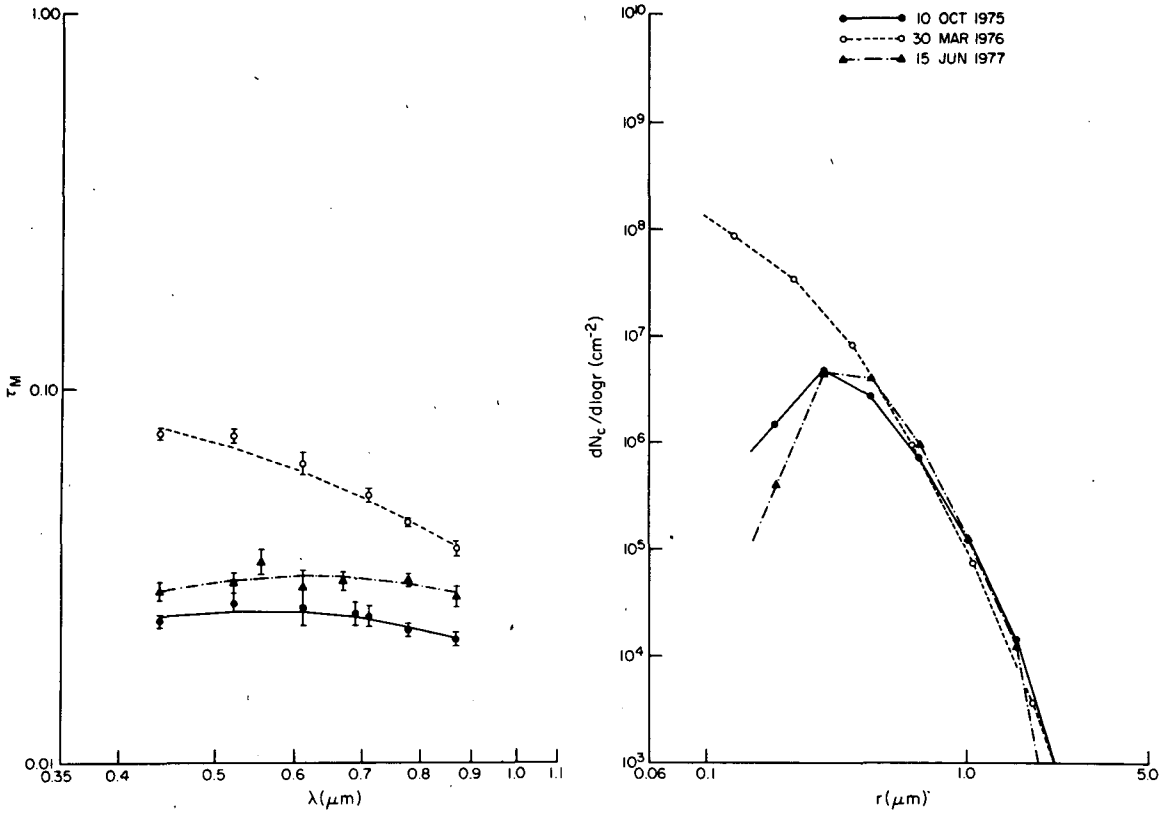

FIG. 5. As in Fig. 2 except for measurements on 10 October 1975, 30 March 1976 and 15 June 1977.

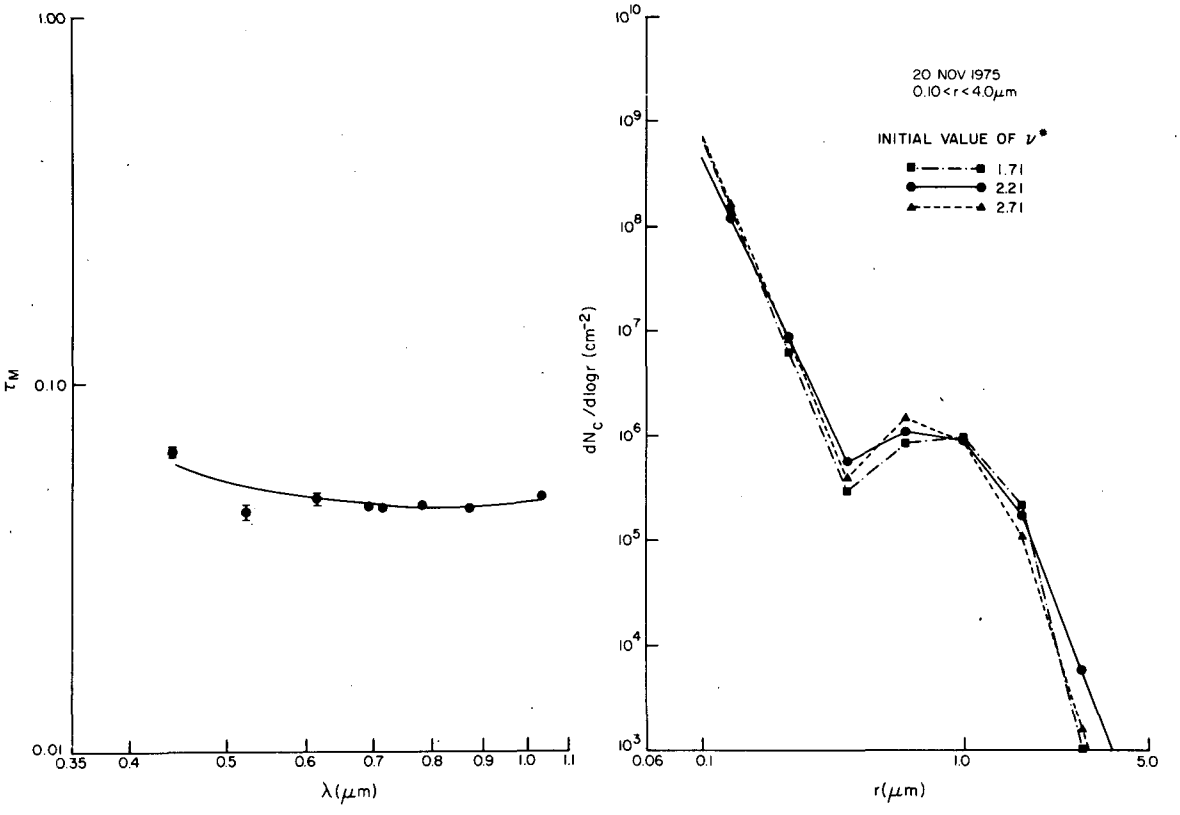

FIG. 6. As in Fig. 1 except for measurements collected on 20 November 1975.

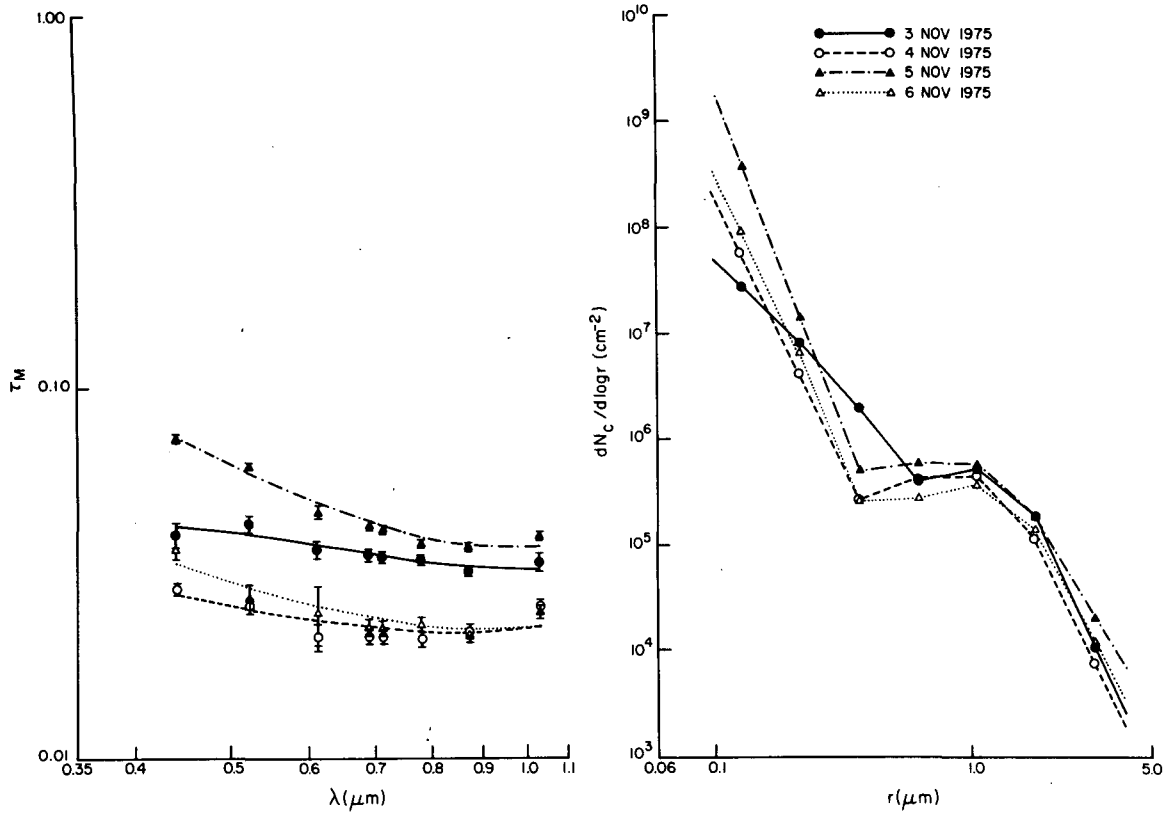

FIG. 7. As in Fig. 2 except for measurements on four consecutive days from 3 to 6 November 1975.

1975, 30 March 1976 and 15 June 1977. On these days (as well as several others) the $\tau_M(\lambda)$ measurements had characteristic negative curvature resulting in size distributions which tended to be peaked but quite broad and asymmetric. There appears to be correspondence between the slope of the $\tau_M(\lambda)$ measurements at the short wavelengths and the radius at which the distribution attains a maximum. The Mie optical depth measurements which produce this second class of distributions (type II) are typically very small [$\tau_M(0.6120\ \mu m) \approx 0.03$] with Ångström turbidity coefficients which are typically negative ($\alpha \approx -0.23$). The single data case of 30 March 1976 (see Fig. 5) deviates the most from these values, and the corresponding size distribution could equally well be categorized as a type I (Junge-type) distribution, thus making classification according to three distinct types somewhat arbitrary.

Perhaps the most interesting distribution type which has been observed thus far is one for which the spectral optical depth values are intermediate between the large turbidities of type I and the small turbidities of type II. On occasions when the Mie optical depths are intermediate in magnitude [$\tau_M(0.6120\ \mu m) \approx 0.05$], $\tau_M(\lambda)$ tends generally to decrease with wavelength ($\alpha \approx 0.5$) but with positive curvature. An example of this type (which will be referred to as type III) is illustrated in Fig. 6 for the data of 20 November 1975. On this day the Ångström turbidity coefficient was estimated to be 0.21, and thus inversions were performed using Junge distribution initial weighting functions with $\nu^* = 1.71$, 2.21 and 2.71. Fig. 6 clearly demonstrates that not only do non-Junge aerosol size distributions result but that the inversion procedure is quite capable of perturbing the initial weighting functions $h^{(0)}(r)$ as required. All days for which the Mie optical depths exhibit relatively small, but positive, Ångström turbidity coefficients with positive curvature imply aerosol size distributions which can be represented as a combination of a power law (type I) and a relatively monodisperse (type II) distribution, as is the case with the data of Fig. 6. These types of distributions have been observed on about 50% of the days examined thus far. It is consistent with the present results, however, to consider types I and II to be subsets of the more general type of distribution shown in Fig. 6 since all distributions can be represented by a combination of types I and II where the relative concentrations of these two types vary in space and time.

Fig. 7 illustrates the spectral optical depth measurements and corresponding aerosol size distributions for an episode of four consecutive days in November 1975. Note in particular that $\tau_M(\lambda)$ for the three longest wavelengths is very similar in shape for all four days as is the size distribution function for the larger particles. However, the slopes of the $\tau_M(\lambda)$ measurements

at the shorter wavelengths are directly correlated with the slopes of the Junge part of the aerosol size distributions at the smaller radii.

The resulting two-component size distributions shown in Figs. 6 and 7 are consistent with the production mechanisms of atmospheric aerosol particles. Those particles with radii $\lesssim 0.5$ μm are produced by a combination of nucleation from the gas phase and subsequent coagulation. Particles having radii $\gtrsim 1.0$ μm are principally the result of mechanical and wind stresses at the earth's surface. It is known from aerosol physics that these production mechanisms are not very effective in the 0.5–1.0 μm range, and thus it is not surprising that a separation of two regions might sometimes be observed. A more complete discussion of aerosol physics can be found in Twomey (1977). A review of the multimodal nature of size distributions and their physical characteristics is given by Whitby (1978).

Curcio (1961) assumed that the atmospheric particulates were composed of such a two-component system with the smaller particles given by a Junge distribution and the larger ones by a Woodcock or Gaussian distribution. Most of the spectral attenuation measurements he presented, as well as theoretical computations using this model, have wavelength characteristics similar to those presented above for wavelengths in the visible and near-infrared regions. Curcio similarly found that the higher attenuation data cases tended to be dominated by Junge-type aerosol size distributions in essential agreement with the results presented above.

Although Yamamoto and Tanaka (1969) inverted data with wavelength characteristics similar to those in Figs. 6 and 7, their inversions show none of the bimodal characteristics which we have observed. This may be partly due to their representing the size distributions on a scale of $n(r)$ or dN/dr, rather than $dN/d\log r$, which tends to stretch the appearance of the distributions.

As pointed out earlier, gradations between clear-cut distribution types occasionally occur, making classification into three distinct categories somewhat arbitrary. Fig. 8 illustrates the spectral optical depth measurements and corresponding size distributions for 1 and 3 November 1976 and 18 May 1977, days for which the aerosol size distributions are very similar and the optical depth data show very subtle curvature differences. In estimating the relative frequencies of abundance, the size distribution for 3 November 1976 was considered to be partly type I and partly type III, while that for 18 May 1977 was considered to be type I. The distribution on 18 May 1977, in particular, could have been placed with some justification in any of the three categories.

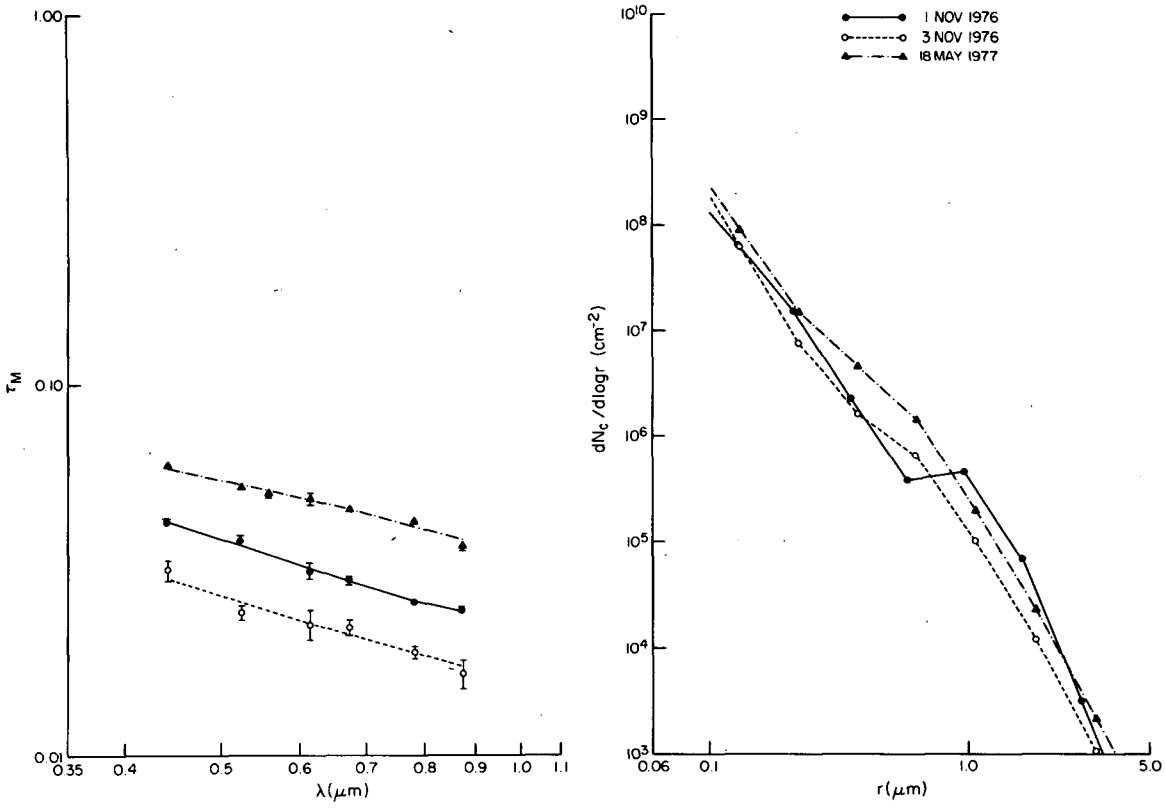

FIG. 8. As in Fig. 2 except for measurements on 1 November 1976, 3 November 1976 and 18 May 1977.

4. Practical considerations

Some of the practical difficulties associated with obtaining satisfactory size distribution determinations from inversion of attenuation coefficients as a function of wavelength or angular scattering intensities as a function of scattering angle have been discussed by various investigators (e.g., Yamamoto and Tanaka, 1969; Dave, 1971). Two aspects of the remote sensing determination of aerosol size distributions, namely, the radii limits of maximum sensitivity and the assumed index of refraction of the atmospheric aerosol particles, are worth reexamining in the context of the present investigation. The necessity of weighting the kernel by a modifying function $h(r)$, as well as the need to scale the Lagrange multiplier γ according to the magnitude of one of the elements of the matrix $\mathbf{A}^T\mathbf{C}^{-1}\mathbf{A}$, has been discussed previously.

In Section 3 it was pointed out that the radius range of the atmospheric particulates which contributes the most significantly to the Mie optical depth measurements is itself a function of the aerosol size distribution to be determined. In order to see why this should be the case, consider the contribution function $\Gamma(r,\lambda)$ defined as

$$\Gamma(r,\lambda)=\pi r^2 Q_{\text{ext}}(r,\lambda,m)\frac{dN_c}{d\log r}. \tag{15}$$

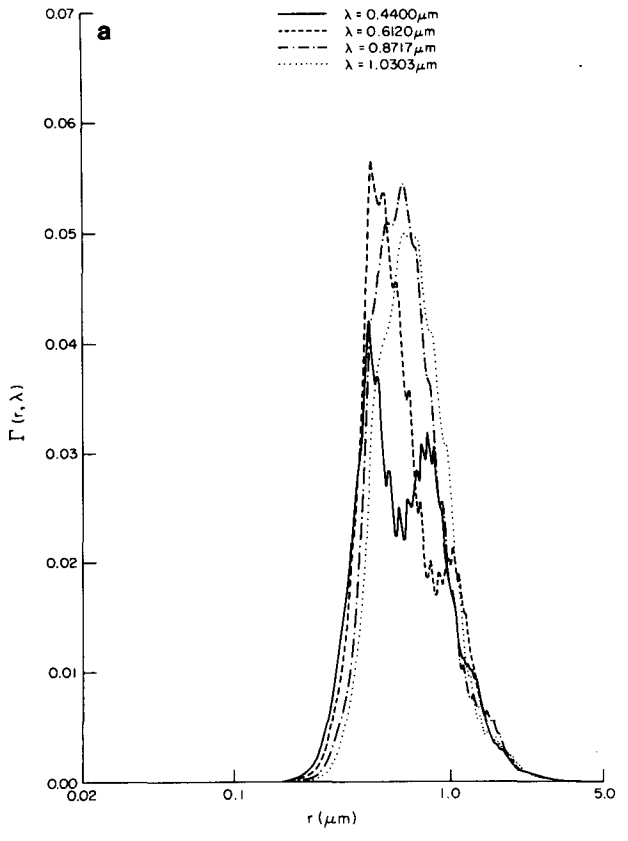

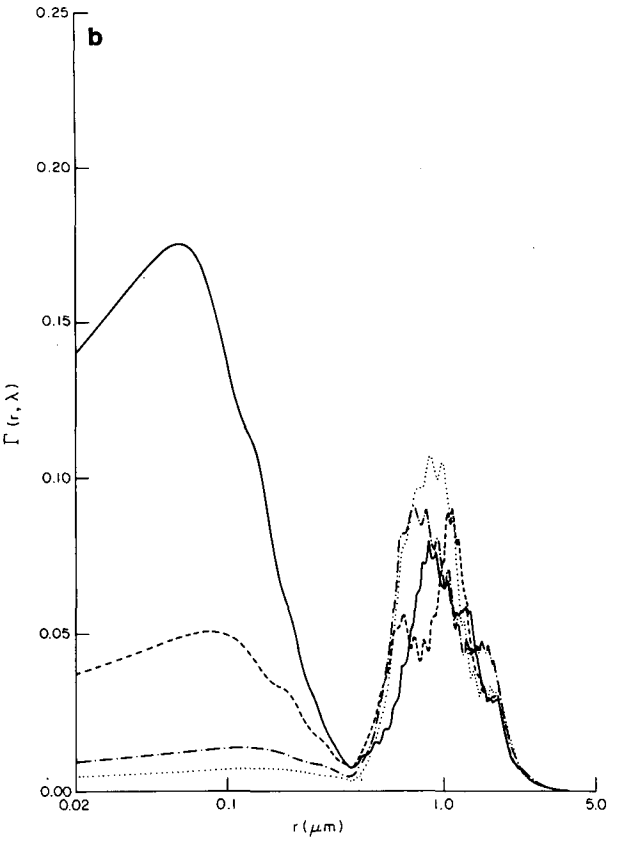

FIG. 9. Contribution function $\Gamma(r,\lambda)$ as a function of $\log r$ and λ for (a) the aerosol size distribution of 24 October 1975 (see Fig. 3) and (b) the aerosol size distribution of 20 November 1975 (see Fig. 6).

With this definition,

$$\tau_M(\lambda)=\int_{\log r_a}^{\log r_b}\Gamma(r,\lambda)d\log r, \tag{16}$$

and thus the integral under a curve of $\Gamma(r,\lambda)$ vs $\log r$ represents the regression fit to the $\tau_M(\lambda)$ measurement for the spectral band which is centered at λ. The contribution function defined here is similar to the probability density function defined by Fraser (1975). However Fraser uses a unit volume particle size distribution based on dN/dr, and normalizes the extinction cross section by the resulting attenuation coefficient.

Fig. 9a illustrates the contribution function $\Gamma(r,\lambda)$ as a function of $\log r$ for the columnar aerosol size distribution of 24 October 1975 ($\nu^*=2.23$ case of Fig. 3) and for four different wavelengths (0.4400, 0.6120, 0.8717 and 1.0303 μm) on this day. Fig. 9a indicates that the radii which contribute to the spectral Mie optical depth measurements on 24 October 1975 are restricted to lie in the range $0.15\ \mu\text{m}\lesssim r\lesssim 3.0\ \mu\text{m}$. With this type of distribution (i.e., type II where τ_M increases with wavelength), it generally follows that the radius

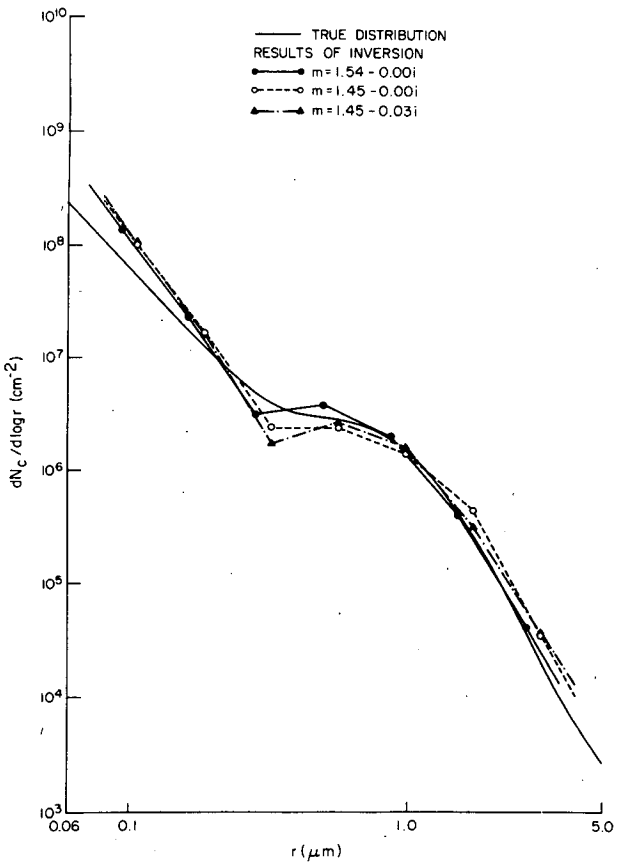

FIG. 10. Inversion solutions obtained for simulated $\tau_M(\lambda)$ data computed for an aerosol size distribution having a combination of Junge plus log-normal composites and a refractive index of $m=1.54-0.00i$. The refractive indices assumed in the inversions are indicated in the figure.

range for which there is significant contribution to the optical depth measurements is more restricted than for other distribution types. Attempting to perform an inversion for radii beyond this sensitive region results in an unstable, highly oscillatory and hence unphysical solution. As a consequence, some trial and error is usually required in order to isolate the proper radius interval. Therefore, for a set of optical depth measurements over a given spectral range, it does not necessarily follow that the upper and lower limits for sensitivity are fixed as implied by Yamamoto and Tanaka (1969) but instead vary, depending on the form of the unknown size distribution.

As an example of this, a very different contribution function is obtained for the more typical composite size distributions having both Junge- and log-normal type components (type III). Fig. 9b illustrates the contribution function for the size distribution of 20 November 1975 ($\nu^*=2.71$ case of Fig. 6). The contribution function in the radius interval $0.4\ \mu\text{m}\lesssim r\lesssim 4.0\ \mu$m is primarily produced by the log-normal part of the aerosol size distribution and therefore has a form similar (although shifted to larger radii) to the contribution function of Fig. 9a. This demonstrates that a distribution with a greater abundance of large particles can have the benefit of extending the range of maximum sensitivity to somewhat larger radii than would otherwise be detectable were the distribution simply Junge with measurements extending only to $\lambda\approx 1.0\ \mu$m. The contribution function at the shorter radii is due primarily to the Junge part of the aerosol size distribution and therefore depends on both the effective ν^* value and the constant of the Junge distribution at these radii. Since the inverted aerosol size distributions for 20 November 1975 (and in fact most distributions of type III) were obtained by assuming a minimum radius of 0.1 μm, the contribution function below 0.1 μm represents only what would be observed were the slope of the Junge part of the size distribution extended to smaller radii. As Fig. 9b illustrates, significant contribution to the optical depth measurements could be produced below 0.1 μm at the shorter wavelengths. However, an integral over the extended radius range of $\Gamma(r,\lambda)$ would produce a wavelength dependence of $\tau_M(\lambda)$ which no longer has the gentle slope with well-developed positive curvature that is observed. This implies that the aerosol size distribution cannot continue with such a large slope (ν^*) for radii $<0.1\ \mu$m but must decrease at some point not far below 0.1 μm. The aerosol size distributions of type III are therefore bimodal with the radius of the first maximum being $\lesssim 0.1\ \mu$m, but with the specific radius being undetectable with spectral attenuation measurements at visible and near-infrared wavelengths.

The bimodal size distributions of type III are not normally as difficult to invert as those of type II but they do have certain idiosyncrasies of their own. If inversions are attempted using an upper radius which is too large (or occasionally too small), instabilities develop such that subsequent iterations produce more and more particles at the larger radii. When this occurs, the number of particles in the region between the Junge and log-normal parts of the size distribution are typically at a minimum. The inversion result within this intermediate region is intrinsically unstable if the number densities are small enough so that little contribution is made to the resultant optical depths. Both instabilities were found to be critically dependent on the value of the upper radius limit. A radius range of $0.1\ \mu\text{m}<r<4.0\ \mu$m is normally the most stable for data of this type (when inverting with $m=1.45-0.00i$). When the proper radius range is isolated, all cases having different initial Junge distribution weighting functions, as well as all iterations within each case, are stable and similar as seen upon examination of Fig. 6.

The sensitivity of the inverted size distribution to index of refraction has been treated analytically by Yamamoto and Tanaka (1969). Using van de Hulst's (1957) anomalous diffraction theory, Yamamoto and Tanaka showed that the inverted aerosol size distributions maintain their *shape* under various indices of

refraction (shifting slightly in both magnitude and radius). Representing the refractive index as a complex number $m=n-\kappa i$ and extending Yamamoto and Tanaka's (1969) results to a scale of $dN_c(r)/d\log r$, it can be shown that

$$\frac{dN_c\left(\frac{0.54r}{n-1}\right)}{d\log r}=\left(\frac{n-1}{0.54}\right)^2\frac{dN_c(r)}{d\log r}. \tag{17}$$

In this expression $dN_c(r)/d\log r$ represents the size distribution obtained for $n=1.54$ and $dN_c[0.54r/(n-1)]/d\log r$ represents the size distribution obtained for a different real refractive index n where the radius is scaled as indicated. [Within the limits of applicability of the anomalous diffraction approximation, this expression is strictly applicable when $\kappa/(n-1)$ is held fixed for both inversions.]

In order to see how well this performs for refractive indices between 1.45 and 1.54, we considered an aerosol size distribution consisting of a combination of Junge and log-normal components for radii between 0.02 and 10.0 μm. Assuming that this distribution function is applicable for $m=1.54-0.00i$, Mie optical depths were then computed at each of seven wavelengths between 0.4400 and 1.0303 μm. These values of $\tau_M(\lambda)$ were used without the addition of random error to determine particle size distributions by the method described in Section 2 for $m=1.54-0.00i$, $1.45-0.00i$ and $1.45-0.03i$. For these inversions, the radii limits differed from that of the true distribution as described by the discussion on radius sensitivity. The results are presented in Fig. 10 where the solid curve represents the assumed model distribution and the broken curves are the results of computation (inversion) for the refractive indices indicated. The spectral optical depth calculations, although not explicitly illustrated, exhibit the characteristic wavelength dependence expected for this type of size distribution (i.e., little wavelength dependence but with positive curvature).

It can be seen on examination of Fig. 10 that the inversion result for the refractive index $m=1.54-0.00i$ agrees very well with the model distribution, particularly for $r\gtrsim 0.16$ μm. This is due to the fact that the refractive index assumed in the model distribution when generating the data is the same as that used in the inversion. The deviation which does occur between the true and computed distribution is due primarily to truncating the lower radius assumed in the inversion (in this case $r_a=0.07$ μm and $r_b=3.5$ μm). Extension of the lower radius much less than that used in this example, however, would lead to instabilities in the inversion.

Fig. 10 suggests that the inverted size distributions obtained when $n=1.45$ (for $r_a=0.08$ μm, $r_b=4.00$ μm) are quite similar regardless of the imaginary part of the complex refractive index (at least when $\kappa\lesssim 0.03$). It is similarly apparent that the *shapes* of the size distributions for $n=1.45$ and $n=1.54$ are similar as suggested by Yamamoto and Tanaka (1969). The reduction in magnitude and the shift to larger radii which does occur as the real part of the refractive index decreases is in essential agreement with that of (17).

Although no random error was added to the simulated measurements, the same set of data was used in performing inversions with all three refractive indices. This type of analysis has been performed for several other types of aerosol size distributions, including Junge and log-normal, and the results indicate that (17) is able to explain the major differences in the inversion for all three refractive indices considered. Additional sensitivity analysis using real data and a wider range of aerosol refractive indices is required to fully examine the problem of potential refractive index biases in the retrieval of aerosol size distribution from spectral attenuation measurements.

The effect of variations of the refractive index with wavelength and/or particle size has not been considered in the present investigation. Although these effects are not expected to be significant for most aerosol systems, one can imagine situations in which these effects can be large. Gillespie *et al.* (1978) considered the effects of an atmospheric aerosol consisting of small particles with one refractive index ($m=1.8-0.5i$) and large and giant particles with another refractive index ($m=1.5-0.0i$). They computed the volume extinction coefficient at three wavelengths between 0.55 and 1.06 μm and compared the results with those of a model with the same size distribution and a single refractive index ($m=1.50-0.005i$). Their results indicate that the difference in the extinction coefficient between the models is small with differences of 15% at 0.55 μm and only 2% at 1.06 μm. This effect would alter slightly the inverted size distribution result of the large aerosol particles ($0.1\lesssim r\lesssim 1.0$ μm) while having little effect on the size distribution of the giant particles ($r\gtrsim 1.0$ μm). For a less dramatic difference in the particulate refractive index with size range the differences in the extinction coefficient (or optical depth) computed with a mean refractive index will be even further reduced.

5. Summary and conclusions

An inversion solution to the linear system of equations $\mathbf{g}=\mathbf{Af}$ has been derived which explicitly considers the magnitude of the standard deviations in a set of measurements $\mathbf{g}$. This formula [Eq. (14)] has been applied to the problem of determining the columnar aerosol size distribution from spectral measurements of the particulate (Mie) optical depth in the wavelength region $0.4400\ \mu\text{m}\leqslant\lambda\leqslant 1.0303\ \mu$m. An iterative method of solution is described whereby an estimate of the size distribution is included in the elements of the $\mathbf{A}$ matrix. With this procedure, the inverted solution vector $\mathbf{f}$

amounts to a modifying function to the assumed form of the size distribution.

As demonstrated by the family of curves in the right portion of Figs. 1, 3 and 6, this iterative algorithm is quite capable of perturbing the initial estimates of the size distribution as required. In all instances three different Junge size distributions had been initially assumed so that the results after subsequent iterations could be intercompared. Tests with both real and generated spectral measurements of the Mie optical depth indicate that this method of solution is quite capable of inverting a wide variety of observation types. The only difficulty which normally arises is in selecting the radius range having the major contribution to the measurements.

The subject of radii limits has been discussed in some detail in Section 4 where it was shown that the radii which contribute most significantly to the magnitude of the Mie optical depth measurements vary somewhat with the type of the size distribution to be retrieved. Satisfactory size distribution determinations can normally be obtained for the radii range $0.10\ \mu m < r < 4.0\ \mu m$ when measurements are available for wavelengths throughout the visible and near-infrared regions. The greatest difficulty arises when the size distribution is a relatively monodisperse distribution contained in a narrow radius interval around 0.5 μm. Uncertainties in the complex refractive index have been found to have little effect on the spectral attenuation problem, particularly with regard to absorption, as illustrated by the family of curves in Fig. 10.

Columnar aerosol size distributions have been determined by inversion of spectral Mie optical depth measurements for 57 days in Tucson, Arizona. The optical depth measurements and corresponding aerosol size distributions are illustrated in Figs. 1–8 for a few of these days. The results generally indicate (at least for $r \gtrsim 0.1\ \mu m$) that the aerosol size distribution on a particular day can be represented either as a Junge distribution (type I), a relatively monodisperse distribution such as a log-normal or gamma distribution (type II), or as a two-component system consisting of a combination of both of these types (type III).

Type I distributions have been observed on 20% of the days examined thus far while types II and III have been observed on approximately 30 and 50% of the days, respectively. The type I distributions occur mainly in the fall and late spring in Tucson when the optical depths are the largest $[\tau_M(0.6120) \approx 0.08]$ and when the spectral optical depth measurements exhibit linear or slightly positive curvature on a $\log\tau_M$ vs $\log\lambda$ scale with relatively steep slopes ($\alpha \approx 1.2$). Type II distributions, on the other hand, occur in the late fall and early summer when the optical depths are the lowest $[\tau_M(0.6120) \approx 0.03]$. Under these circumstances $\tau_M(\lambda)$ tends generally to increase with wavelength ($\alpha \approx -0.2$) while exhibiting negative curvature on a $\log\tau_M$ vs $\log\lambda$ scale. The size distributions of type III occur throughout the winter months when virtually no distributions of types I and II occur. These distributions occur when the optical depths are intermediate in magnitude $[\tau_M(0.6120) \approx 0.05]$, the Ångström slope $\alpha \approx 0.5$, and the $\log\tau_M$ measurements show positive curvature as a function of $\log\lambda$ particularly at the longer wavelengths. Both the distributions and the optical depths of this type appear to be combinations of types I and II.

Curcio (1961) found that the majority of his observations of attenuation coefficient along a horizontal path in the Chesapeake Bay area could best be described as resulting from a combination of type I and type II distributions (i.e., type III). He also determined that larger optical depths resulted from Junge-type size distributions. This is in support of the results obtained in the present investigation for vertical attenuation at a different location. Rangarajan (1972) investigated the Ångström wavelength exponent for 520 observations at Poona, India. His results are in agreement with those reported here in that the lowest (near zero) α values occurred on occasions of lowest turbidity. Rangarajan's (1972) median value of 0.5 is the same as our type III distributions, those found to occur the most frequently.

Acknowledgments. The research reported in this article has been supported by the National Science Foundation under Grants DES75-15551 and ATM75-15551-A01 and the Office of Naval Research under Grant N00014-76-C-0438.

REFERENCES

Ångström, A., 1929: On the atmospheric transmission of sun radiation and on dust in the air. *Geogr. Ann.*, **11**, 156–166.

Curcio, J. A., 1961: Evaluation of atmospheric aerosol particle size distribution from scattering measurements in the visible and infrared. *J. Opt. Soc. Amer.*, **51**, 548–551.

Dave, J. V., 1971: Determination of size distribution of spherical polydispersions using scattered radiation data. *Appl. Opt.*, **10**, 2035–2044.

Fraser, R. S., 1975: Degree of interdependence among atmospheric optical thicknesses in spectral bands between 0.36–2.4 μm. *J. Appl. Meteor.*, **14**, 1187–1196.

Gillespie, J. B., S. G. Jennings and J. D. Lindberg, 1978: Use of an average complex refractive index in atmospheric propagation calculations. *Appl. Opt.*, **17**, 989–991.

Grassl, H., 1971: Determination of aerosol size distributions from spectral attenuation measurements. *Appl. Opt.*, **10**, 2534–2538.

Herman, B. M., S. R. Browning and J. A. Reagan, 1971: Determination of aerosol size distributions from lidar measurements. *J. Atmos. Sci.*, **28**, 763–771.

Junge, C. E., 1955: The size distribution and aging of natural aerosols as determined from electrical and optical data on the atmosphere. *J. Meteor.*, **12**, 13–25.

——, 1963: *Air Chemistry and Radioactivity.* Academic Press, 382 pp.

King, M. D., and D. M. Byrne, 1976: A method for inferring total ozone content from the spectral variation of total optical depth obtained with a solar radiometer. *J. Atmos. Sci.*, **33**, 2242–2251.

Knestrick, G. L., T. H. Cosden and J. A. Curcio, 1962: Atmospheric scattering coefficients in the visible and infrared regions. *J. Opt. Soc. Amer.*, **52**, 1010–1016.

Liebelt, P. B., 1967: *An Introduction to Estimation Theory.* Addison–Wesley, 273 pp.

Phillips, D. L., 1962: A technique for the numerical solution of certain integral equations of the first kind. *J. Assoc. Comput. Mach.*, **9**, 84–97.

Quenzel, H., 1970: Determination of size distribution of atmospheric aerosol particles from spectral solar radiation measurements. *J. Geophys. Res.*, **75**, 2915–2921.

Rangarajan, S., 1972: Wavelength exponent for haze scattering in the tropics as determined by photoelectric photometers. *Tellus*, **24**, 56–64.

Reagan, J. A., J. D. Spinhirne, D. M. Byrne, D. W. Thomson, R. G. dePena and Y. Mamane, 1977: Atmospheric particulate properties inferred from lidar and solar radiometer observations compared with simultaneous *in situ* aircraft measurements: A case study. *J. Appl. Meteor.*, **16**, 911–928.

Shaw, G. E., J. A. Reagan and B. M. Herman, 1973: Investigations of atmospheric extinction using direct solar radiation measurements made with a multiple wavelength radiometer. *J. Appl. Meteor.*, **12**, 374–380.

Twomey, S., 1963: On the numerical solution of Fredholm integral equations of the first kind by the inversion of the linear system produced by quadrature. *J. Assoc. Comput. Mach.*, **10**, 97–101.

——, 1965: The application of numerical filtering to the solution of integral equations encountered in indirect sensing measurements. *J. Franklin Inst.*, **279**, 95–109.

——, 1977: *Atmospheric Aerosols. Developments in Atmospheric Science*, Vol. 7, Elsevier, 302 pp.

van de Hulst, H. C., 1957: *Light Scattering by Small Particles.* Wiley, 470 pp.

Whitby, K. T., 1978: The physical characteristics of sulfur aerosols. *Atmos. Environ.*, **12**, 135–159.

Yamamoto, G., and M. Tanaka, 1969: Determination of aerosol size distribution from spectral attenuation measurements. *Appl. Opt.*, **8**, 447–453.